Quantum Chemical Molecular Dynamics Simulation of Single-Walled Carbon Nanotube Cap Nucleation on an Iron Particle

Yasuhito Ohta,[†,⊥] Yoshiko Okamoto,[†] Alister J. Page,[†] Stephan Irle,[†,‡,*] and Keiji Morokuma[†,§,*]

[†]Fukui Institute for Fundamental Chemistry, Kyoto University, Kyoto 606-8103, Japan, [‡]Institute for Advanced Research and Department of Chemistry, Nagoya University, Nagoya 464-8602, Japan, and [§]Cherry L. Emerson Center for Scientific Computation and Department of Chemistry, Emory University, Atlanta, Georgia 30322. [⊥]Present address: Department of Chemistry, Nara Women's University, Nara 630-8506, Japan.

ABSTRACT The atomic scale details of single-walled carbon nanotube (SWNT) nucleation on metal catalyst particles are elusive to experimental observations. Computer simulation of metal-catalyzed SWNT nucleation is a challenging topic but potentially of great importance to understand the factors affecting SWNT diameters, chirality, and growth efficiency. In this work, we use nonequilibrium density functional tight-binding molecular dynamics simulations and report nucleation of sp^2-carbon cap structures on an iron particle consisting of 38 atoms. One C_2 molecule was placed every 1.0 ps around an Fe_{38} cluster for 30 ps, after which a further 410 ps of annealing simulation without carbon supply was performed. We find that sp^2-carbon network nucleation and annealing processes occur in three sequential and repetitive stages: (A) polyyne chains on the metal surface react with each other to evolve into a Y-shaped polyyne junction, which preferentially form a five-membered ring as a nucleus; (B) polyyne chains on the first five-membered ring form an additional fused five- or six-membered ring; and (C) pentagon-to-hexagon self-healing rearrangement takes place with the help of short-lived polyyne chains, stabilized by the mobile metal atoms. The observed nucleation process resembles the formation of a fullerene cage. However, the metal particle plays a key role in differentiating the nucleation process from fullerene cage formation, most importantly by keeping the growing cap structure from closing into a fullerene cage and by keeping the carbon edge "alive" for the addition of new carbon material.

KEYWORDS: quantum chemical molecular dynamics simulations · density functional tight binding · self-assembly · continued carbon nanotube growth · iron catalyst nanoparticle · nonequilibrium dynamics

Numerous experimental and theoretical efforts aimed at understanding the mechanisms of nucleation and growth of single-walled carbon nanotubes (SWNTs) on metal nanoparticles have been reported.[1−5] However, the nonequilibrium processes driving the transformation of molecular carbon feedstock species into an initial sp^2-carbon network, as well as the growth of the network into a SWNT, remain unclear. Many parameters that influence these processes, including temperature, the type of carbon feedstock, supply rate, catalyst type, particle size, addition of reducing agents, *etc.*, have been probed experimentally. Recent remarkable environmental transmission electron microscopy (ETEM) studies have also shown time-resolved details of metal-catalyzed SWNT nucleation and growth at the atomic level.[6,7] However, current TEM resolution is still not good enough to observe atomic scale *dynamics*. Moreover, experimental findings appear to be contradictory and/or highly system-dependent, particularly regarding carbide formation and the melting of metal nanoparticles. Thus, atomic scale knowledge of the nucleation process remains elusive yet seems to be a prerequisite toward the ultimate goal of chirality- and diameter-selective (*n*,*m*) SWNT synthesis.

As for computational chemistry modeling, molecular dynamics (MD) simulations of metal-catalyzed SWNT nucleation and growth processes remain a challenge. However, they exhibit the potential to yield atomic level details of the carbon−catalyst interplay. With very few exceptions, MD simulations of SWNT synthesis reported thus far have employed variations of Brenner's reactive empirical bond order (REBO) potential,[8−11] which is a classical potential based on the molecular mechanics concept. However, such REBO/MD simulations have never produced substantial SWNT growth without forcibly injecting feedstock carbons inside the metal cluster center, and even SWNTs grown in this artificial manner possess side walls that are highly defective.[9] Since REBO-based approaches do not explicitly take into account the quantum mechanical nature of electrons, such as π conjugation and the aromatic stabilization effects of carbon, the

*Address correspondence to sirle@iar.nagoya-u.ac.jp, morokuma@fukui.kyoto-u.ac.jp.

Received for review July 11, 2009 and accepted September 25, 2009.

Published online October 14, 2009. 10.1021/nn900784f CCC: $40.75

delicate charge balance between carbon and metal, or the effect arising from near-degeneracy of d-orbital of metal, it is evident that the serious deficit observed in the REBO-based SWNT growth simulations is related to their inability to describe the evolution and electronic structure of the catalyst and SWNT during nucleation and growth.[12] Even in carbon-only systems, such as fullerenes, we have found that the formation dynamics observed in REBO-based MD simulations differs greatly from that obtained using QM/MD simulations.[13]

Two studies that have employed a first-principles quantum chemical MD technique based on density functional theory (DFT) (*viz.* the popular Car−Parrinello approach (CPMD)) for the simulation of SWNT nucleation stand out.[14,15] However, due to the high computational cost of DFT-based CPMD, these simulations have been limited to few picosecond (ps) time scales and are therefore too short to explore relevant dynamics. At present, DFT-based CPMD does not provide a viable alternative to REBO/MD simulations.

The density functional tight-binding (DFTB) method is an approximate DFT method where Hamiltonian and overlap matrix elements are determined by a parametrization procedure based on the two-center approximation using density functional calculations.[16−18] We have recently compared the results of DFTB with those obtained from calculations for the metal−carbon adhesion energy of a nanotube−metal cluster.[19] It turned out that the difference between DFTB and DFT results is practically small enough for implementing high-temperature molecular dynamics simulations of the metal−carbon systems. The DFTB-based quantum chemical MD (QM/MD) approach is 100−1000 times faster than conventional DFT-based CPMD yet provides comparable accuracy in the description of metal-attached carbon clusters. With respect to DFTB/MD simulations of SWNT growth, we have recently studied the mechanism of continued SWNT growth on metal catalyst particles and have successfully shown how an sp^2-carbon network (fragment, cap or preattached SWNT) grows into a SWNT by reaction of carbon fragments at the Fe−C boundary, either by direct collision or by diffusion.[20−22] However, these studies, which employed time scales of up to 100 ps, did not address the earliest stage of the nanotube growth, namely, the nucleation of the sp^2 network itself by carbon supply to a clean metal cluster catalyst. This was primarily due to the fact that nucleation "from scratch" is considered to be less straightforward than the growth processes discussed above. Recent ETEM images clearly captured carbon cap formation on the metal particle during SWNT growth, although the metal−carbon dynamics during such cap formation is still unclear. Because of this observation, we consider the whole SWNT growth process in the two stages. The first stage is the cap formation from the interaction of carbon feedstock with metal particle, and the second stage is the subsequent continued growth from the generated carbon cap on the metal surface. Our previous studies were limited to the second stage because of demanding computational cost.

Here, we focus on the initial stage, that is, the cap formation process on the metal particle. We report the first QM/MD simulation of SWNT nucleation processes on an Fe particle over a relevant time scale of several hundred picoseconds, using the DFTB method. It is found that five-membered ring formation preferentially occurs first, before being followed by pentagon-to-hexagon self-healing rearrangement in the early stage of nucleation process. The latter has never been observed in the nucleation simulations implemented by other groups. The observed nucleation process resembles the formation of a fullerene cage. However, the metal particle plays a key role in differentiating the nucleation process from fullerene cage formation. Connecting the present nucleation simulation to previous growth simulations,[20−22] albeit piecewise, we show that carbon feed (C or C_2) can form a carbon cap structure on the transition metal cluster, and that the cap can grow into a carbon nanotube.

Model System and Nonequilibrium Molecular Dynamics. As in our previous simulations, we first prepared an iron nanoparticle composed of 38 iron atoms as the metal catalyst. The initial configuration of the Fe_{38} cluster is characterized by a face-centered cubic truncated octahedron arrangement[23] analogous to γ-iron, a stable phase in bulk iron between 1184 and 1665 K.[24] The Fe_{38} cluster was first annealed at a nuclear temperature of 1500 K for 10 ps, after which 10 geometries and associated velocities were randomly extracted from all structures observed between 5 and 10 ps. These geometries and velocities were then used as the starting points for the nonequilibrium carbon-supply simulations and are referred to using Arabic bold numerals **1** to **10**. Each simulation was composed of two steps: (i) 30 ps C_2 supply simulations around the iron cluster, followed by (ii) 410 ps annealing simulations. In step (i), one C_2 molecule was placed around the Fe_{38} cluster at 1.0 ps intervals. It is assumed here that C_2 itself was generated by the decomposition of a carbon precursor, such as acetylene or ethylene, or by vaporization of graphite using arc discharge or laser ablation techniques. The velocity vectors of the C_2 constituent atoms were directed to the center of mass of the Fe_{38} cluster with magnitudes satisfying a Maxwell−Boltzmann distribution at 1500 K. After 30 ps of C_2 supply, the "simulation clock" was reset to zero in step (ii), and a further 410 ps of simulation was performed without supplying any feedstock carbons around the iron cluster. Thus, the spontaneous reaction dynamics of the prepared metal−carbon systems could be focused upon.

RESULTS AND DISCUSSION

C_2 Supply Simulations around the Iron Cluster. In the course of the C_2 supply simulations at 1500 K, incoming C_2 molecules were promptly captured by the iron surface without dissociation from the iron cluster. The C_2 molecules subsequently underwent surface diffusion and polymerized efficiently, quickly forming longer polyyne chains (see Supporting Information Video 1). Figure 1 shows snapshots of the 10 trajectories after 30 ps of C_2 supply simulation. It is clear that the polyyne chains preferentially built Fe−C_n−Fe bridging structures, while the iron cluster somewhat disintegrated due to the increasing C−Fe interaction. We note that *no polygonal rings were formed* during the 30 ps period of C_2 supply simulations.

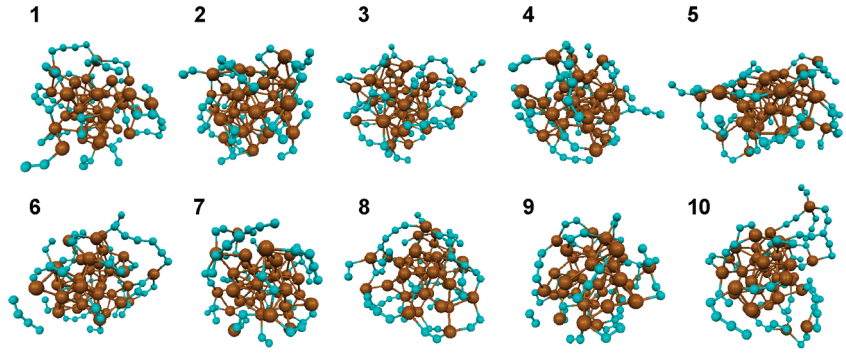

Figure 1. Snapshots of 10 trajectories after 30 ps C_2 supply simulation at 1500 K. Cyan and brown spheres represent carbon and iron atoms, respectively.

During the simulations, the decomposition of C clusters into C atoms was hardly observed, indicating that the dissociation process of C clusters on the metal surface is highly endothermic. Because of this less dissociative behavior of C clusters, we did not observe noticeable penetration of C feedstock into the Fe nanoparticle. This observation should be compared with that obtained from our recent SWNT growth simulations using C *atoms* as feedstock, where penetration of C atoms into the Fe nanoparticle was intermittently observed, although it was a relatively rare event.[22] Our results imply that presence of other atomic or molecular species plays an important role in promoting the decomposition of carbon feedstock on the metal surface.

Carbon Nucleation Simulations. Figure 2, extracted from trajectory **10**, illustrates carbon condensation dynamics typically observed on the iron surface at 1500 K. Initially, at around time $t = 0$ (Figure 2a, which is equivalent to the geometry after 30 ps C_2 supply simulation in Figure 1, structure **10**), the generated polyyne chains performed "snake-like" sinusoidal wave movements, drifted on the iron surface, and thus experienced frequent C−Fe bond breaking and formation. The first created sp^2-carbon polygon was a pentagon, formed at time $t = 18.4$ ps by the cyclization of two carbon chains on the iron surface over a hollow metal site (Figure 2b; see also Supporting Information Video 2). The five-membered ring fragment thus generated was anchored on the iron particle by the interaction between polyyne chains that branched off from the pentagon and iron atoms. At $t = 19.3$ ps, two polyyne chains, remainders of the original two polyyne chains extending from adjacent pentagon sites, soon followed suit to create a hexagon. This resulted in the formation of an indene-like (fused five−six-membered ring) carbon structure, which was anchored to the iron particle by a total of five carbon branches. The Csp^2−Csp^2 bridge fusing the two rings was located on top of the hollow metal position (Figure 2c; see also Supporting Information Video 2). Three five-membered rings were generated sequentially (at $t = 20.5$, 30.4, and 62.9 ps) at different sites of the indene-like carbon fragment by the incorporation of polyyne chains branching out from the indene structure (Figure 2d). The resulting three fused five-membered rings ob-

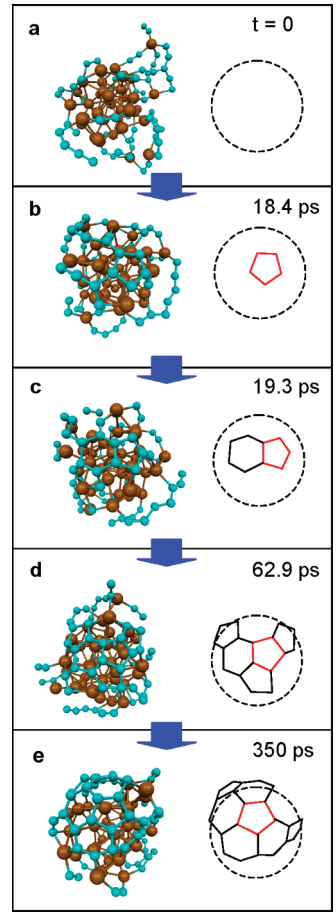

Figure 2. An sp^2-carbon network nucleation process on the iron surface during 350 ps annealing molecular dynamics simulation at 1500 K. Cyan and brown spheres represent carbon and iron atoms, respectively. The snapshots were extracted from trajectory 10: (a) at time $t = 0$, after 30 ps C_2 supply simulation (this snapshot is identical to structure 10 in Figure 1); (b) at $t = 18.4$ ps; (c) at $t = 19.3$ ps; (d) at $t = 90.9$ ps; (e) at $t = 350$ ps. The wireframe polygonal rings depicted on the circle drawn by the dashed line represent the largest polycyclic carbon cluster on the iron surface where the first created five-membered ring is highlighted in red.

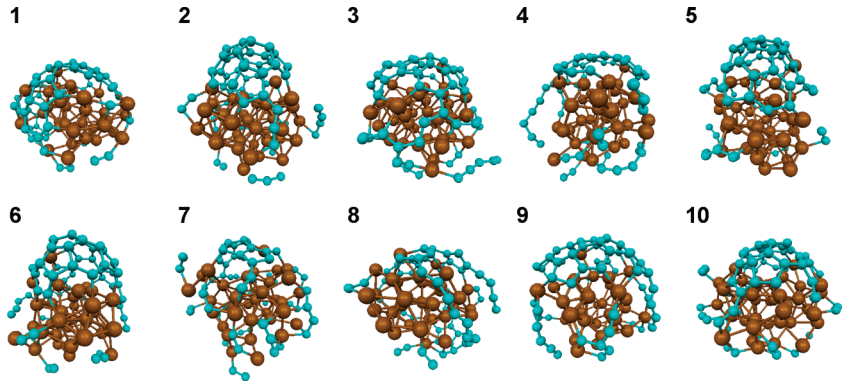

Figure 3. Snapshots of 10 trajectories after 410 ps annealing simulations of the $Fe_{38}C_{60}$ cluster at 1500 K. Cyan and brown spheres represent carbon and iron atoms, respectively.

served at 62.9 ps clearly violate the so-called isolated pentagon rule (IPR).[25] In the subsequent annealing process, it was observed that this pentagon-rich polycyclic cluster experienced occasional ring cleavage due to the interaction of rim carbons with surface iron atoms, leading to the generation of short-lived five-, six-, and seven-membered rings. Scission of a C−C bond in a five-membered ring at the rim of the polycyclic cluster was also observed, generating short polyyne chains as a result. The thermal fluctuation of these polyyne chains led to structural rearrangement of their constituent carbons, thus stabilizing the system by forming additional six-membered rings (see Supporting Information Video 3). By $t = 350$ ps, the original pentagon was surrounded by four six-membered rings (Figure 2e). The transformation from pentagon-rich to hexagon-rich structure observed in our simulations clearly demonstrates the importance of a self-healing mechanism involved in the nucleation of an sp^2-carbon network.

Figure 3 shows snapshots of the 10 trajectories after 410 ps of annealing simulation. In almost all trajectories, polycyclic carbon structures were formed on the iron surface. In trajectories **2**, **5**, **6**, and **10**, the curvature and size of these polycyclic structures were large enough for them to be considered as "carbon cap" fragments. In addition, each structure contained a minimum unit consisting of a single pentagon surrounded by five hexagonal rings (see Supporting Information Video 4 for trajectory **5**) as observed experimentally, for instance by Yoshida *et al.*[7] It is evident that, initially, polyyne-rich metal−sp-carbon clusters spontaneously evolved into a segregated sp^2-carbon cap fragment on the iron surface, without major carbide formation on the surface of the metal particle.

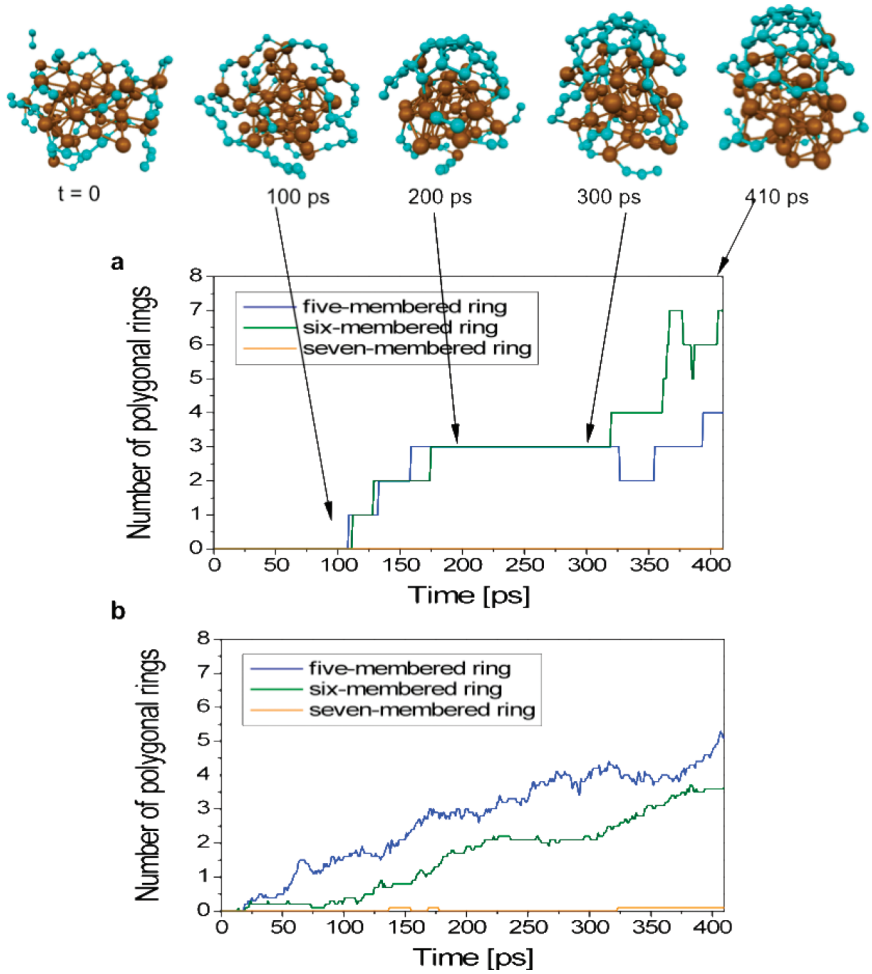

Figure 4. Time variation of the number of polygonal rings during carbon cap formation. (a) Trajectory 10. (b) Averaged over all 10 trajectories.

In the cap Fe clusters **2**, **5**, **6**, and **10**, the diameters of the rim of the carbon caps are comparable with those of the Fe clusters. With the focus on their contact area between the carbon cap and the Fe cluster, the strong σ bonds are made between the Fe atoms located at the outer peripheral edge and the carbon atoms at the rim of the carbon cap. From this observation, it can be expected that the diameter of SWNT increases with the size of metal nanoparticle, although further investigation using different cluster size is necessary.

Ring Condensation Dynamics and Cap Formation. The snapshots in Figure 4 show details of the ring condensation process of trajectory **5**, in terms of ring number statistics for this trajectory (Figure 4a), and ring number statistics averaged over all 10 trajectories (Figure 4b). The ring condensation dynamics in Figure 4a clearly indicates that five- and six-mem-

bered rings are primary components of the polycyclic sp^2-carbon fragment during carbon cap formation on the iron cluster. This feature is consistent with our previous metal-catalyzed SWNT growth simulations, in which a SWNT cap fragment (attached to the Fe_{38} cluster) extended its carbon side wall *via* the incorporation of surface carbons into its metal-anchored edge, forming five- and six-membered rings.[22] As was the case with metal-catalyst-free fullerene nucleation,[13] five-membered rings were preferentially formed during the initial stage of the ring condensation process, as illustrated in Figure 4b. In fact, *in all trajectories, a five-membered ring was the first sp^2-carbon structure generated on the iron surface*. This preferential five-membered ring formation will be explained in the next paragraph. The longevity of these pentagons is related to their higher stability on the convex surface of the iron cluster, which is caused by the curvature imposed by the small-diameter metal particle.[2] In the following paragraph, we divide typical sp^2-carbon network nucleation and annealing processes into three sequential and repetitive stages (A, B, and C) and discuss each in detail.

Figure 5a depicts schematically the typical steps encountered in each stage of the nucleation process. In the first stage, A, the mobility of polyyne chains on the iron surface is lower compared to atomic carbon or C_2 units, but they are nevertheless capable of approaching each other by way of snake-like sinusoidal movements over fluctuating iron sites. In step 1, short polyyne chains are formed on the surface of the iron cluster by the coupling of surface carbon clusters. In step 2, a polyyne chain attaches to another polyyne chain to form a polyyne Y-structure, with its newly generated trivalent sp^2-carbon playing an important role to serve as the "cornerstone" for further cyclization of the two branches. In step 3, branched chains occasionally approach each other by their Brownian surface diffusion, and in step 4, a new C−C bond is created between the two branches of the Y-structure. The distance between the two polyyne branches of the Y-structure is shorter between the second atoms of each branch. Therefore, there is a greater possibility of bond formation here, leading preferentially to the formation of a five-membered ring, than between the second and third atoms leading to a six-membered ring (see (i) and (ii) in Figure 5b). In stage B, steps 1−3 lead to the formation of a five- or six-membered ring fused to the initial pentagon. In step 1, the initial five-membered ring created on the iron surface retains polyyne chains left over from the polyyne collision process. In step 2, two polyyne chains branching off from adjacent sites on the pentagon occasionally approach each other by large-amplitude wave-like vibrations. In step 3, a new C−C bond is formed between the polyyne chains, completing the formation of pentagon or hexagon fused to a pentagon. In this last step (depicted in Figure 5 (iii) and (iv)), two carbon cornerstone atoms (red C's) on

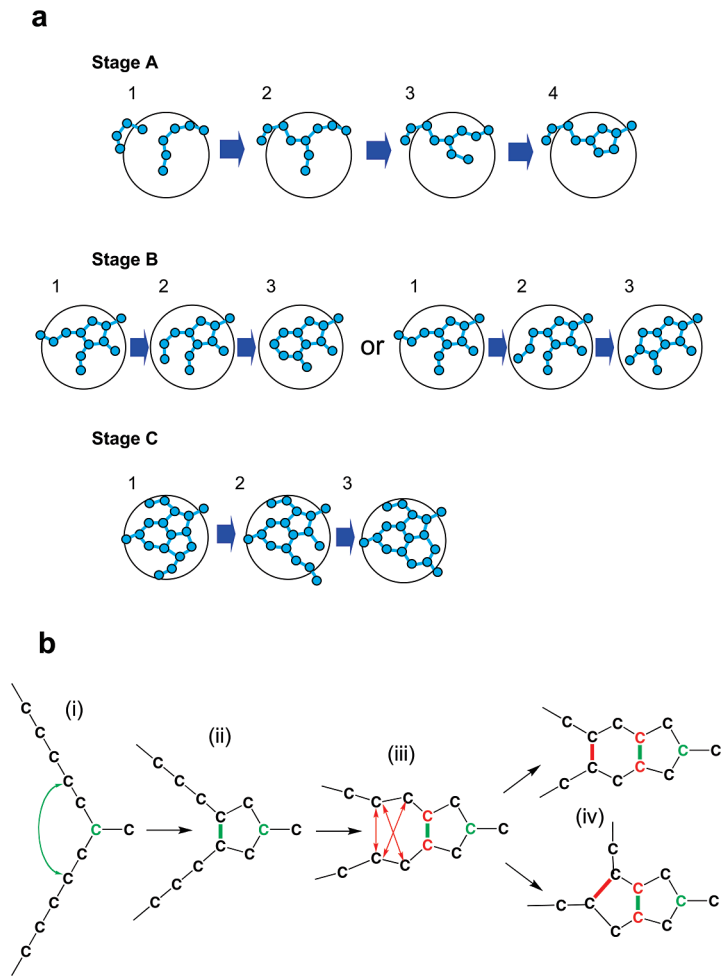

Figure 5. Schematic depiction of the cap formation process on the iron particle. (a) Three stages to form a three-fused polygonal ring complex. Cyan spheres and the white circle represent carbon atoms and the iron particle, respectively. Stage A: Five-membered ring formation initiated by the coupling reaction of polyyne chains on the iron surface. Stage B: Six- or five-membered ring formation fused to a pentagon. Stage C: Pentagon-to-hexagon rearrangement. (b) Carbon polyyne dynamics on the iron particle leading to the formation of pentagon and fused ring structures. Initial pentagon formation from Y-junction (single sp^2 cornerstone, green), and subsequent formation of a pentagon or hexagon fused to the initial pentagon (two sp^2 cornerstones, red).

the original five-membered ring with sp^2-hybridization imposing bond angles close to 120° force formation of pentagon or hexagon during vibrations of the attached polyynes. We note that, as with fullerene cage self-assembly,[13] polycyclic carbon clusters always retained branched polyyne chains, and that these carbon chains contributed not only to the metal anchoring of the sp^2-carbon cluster but also to the extension of the growing sp^2-carbon network. In stage C, pentagon-to-hexagon rearrangement (self-healing) from the polycyclic carbon cluster with adjacent pentagons during the sp^2-carbon network nucleation process is observed. In step 1, the polycyclic carbon cluster possesses several polyyne chains at its rim area, and in step 2, the cluster experiences intermittent breaking of a C−C bond of a pentagon at the rim due to the interaction with iron atoms, leading to the formation of polyyne chains. In

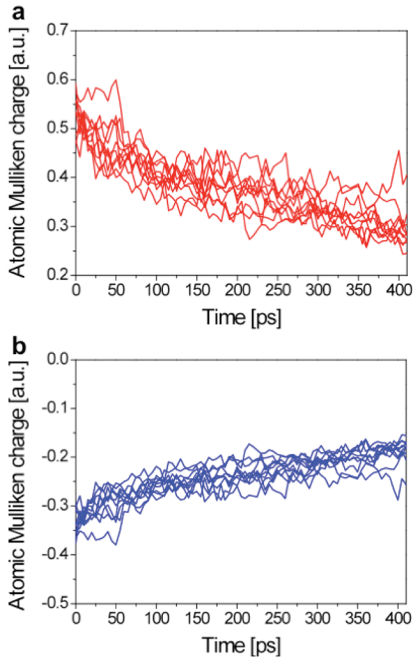

Figure 6. Monitoring of the metal−carbon interaction dynamics. Time evolution of atomic Mulliken charge: for 10 annealing trajectories averaged over (a) iron and (b) carbon atoms.

step 3, these polyyne chains occasionally approach each other and reconnect, forming a new C−C bond, typically forming a new hexagon rather than a pentagon. This preference results partially from the thermodynamic instability of fused pentagons (compared to a fused pentagon−hexagon structure) due to the higher ring strain exhibited by the former and partially from simple geometry arguments as lined out above. Stages A, B, and C take place repeatedly during the cap formation process. The incorporation of surface carbon chains into the polycyclic carbon cluster to form the pentagon-rich sp^2 network, followed by five-to-six-membered ring rearrangement, allows the cluster to slowly turn into a hexagon-rich cluster during the nucleation process.

Stages A, B, and C have close parallels to the nucleation and growth process of fullerene cages, described by us earlier in ref 13. However, the metal particle plays a key role in differentiating the nucleation process from fullerene cage formation. In particular, the metal particle (1) holds carbon fragments on the surface, (2) slows down diffusion, (3) makes the Fe−C bond the most reactive, (4) slows down bond rearrangement processes compared to carbon-only systems, and (5) prevents closure of the curved open-ended carbon structure.

Metal−Carbon Interaction Dynamics during Nucleation Simulations. Figure 6 shows the time variation of Mulliken atomic charge. At $t = 0$, averages of carbon and iron atomic charge were −0.34 and 0.53e, respectively. This charge polarization arises from the back-donation of electrons from iron to carbon, which results in initially weakened Fe−Fe bonds due to electron depletion in the iron system. This explains the initial tendency of the iron cluster to disintegrate. The charge polarization feature observed here is consistent with results obtained from first-principles DFT calculations on model SWNT−metal cluster compounds.[26] However, the degree of the charge polarization decreases with increasing annealing time because carbon atoms covering the metal surface at $t = 0$ gradually coagulate, forming carbon clusters and thus reducing the area of metal−carbon interface.

SUMMARY AND CONCLUSION

The molecular dynamics simulations presented in this work have elucidated the atomistic reaction mechanism in the initial stage of sp^2-carbon network nucleation on a small iron cluster after the supply of C_2 molecules. At first, C_2 units polymerized to form sp-carbon polyyne chains, which moved over the surface by snake-like sinusoidal movement. Polyyne chains collided and initially created a Y-shaped branched polyyne with a single sp^2-carbon center. A C−C bond was then formed between Y-shaped branches, preferentially creating a pentagon as the first ring structure, over a hollow metal site. Branches on the pentagon from the original polyyne chains rapidly cross-networked, primarily producing fused hexagon−pentagon pairs, and also some pentagon−pentagon pairs. This indene-like carbon structure was anchored to the metal particle by attached polyyne chains, with the Csp^2−Csp^2 fusing bond on top of the hollow metal site. Intermittent ring cleavage/reformation of the polycyclic sp^2-carbon network during the nucleation simulation explains the temporary disappearance of carbon cages on the iron particle, as observed in *in situ* ETEM experiments.[7] The pentagon-to-hexagon rearrangement in the border regions of the polycyclic sp^2-carbon fragment observed here clearly demonstrates that a proper pentagon/hexagon ratio can be achieved from an initially pentagon-rich structure. We note that this kind of pentagon-to-hexagon rearrangement has never been observed before in nucleation simulations based on classical molecular dynamics approaches.

As discussed in the introduction, we have previously shown how an sp^2-carbon network (fragment, cap or preattached SWNT) grows into a SWNT by reaction of carbon fragments at the Fe−C boundary by direct collision or diffusion.[20−22] Thus, we have now shown, albeit piecewise, that carbon feed (C or C_2) can form a carbon cap structure on the transition metal cluster, and that the cap structure can subsequently grow into a carbon nanotube. Of course, it is most desirable to continue the present simulations with more carbon supply over longer time periods (*i.e.*, the order of nanoseconds) to demonstrate complete nanotube growth in a single, continuous trajectory. This has not been accomplished yet, but we feel confident that this will be achieved in the future.

The demonstration of pentagon-to-hexagon rearrangement in the cap formation has an important implication with respect to the SWNT growth process. In our previous simulations of continued SWNT growth from both a prepared nanotube placed on a metal cluster[20,21] and a prepared carbon cap,[22] we have shown that the SWNTs produced are very rich in defects, usually exhibiting many pentagons in the side wall structure. It is natural therefore to assume that similar pentagon-to-hexagon rearrangement is likely to take place during SWNT growth, thereby making the SWNT a hexagon-rich structure with a "smooth" carbon side wall. Thus, this pentagon-to-hexagon rearrangement is likely to be a primary mechanism of "defect repair". During SWNT growth, we surmise that defect-rich growth and defect repair take place simultaneously, yielding a near-perfect SWNT. SWNT growth itself is fast, as long as sufficient carbon density is provided, yet SWNT repair is very slow. Much lower carbon supply rates (and hence longer MD trajectories) must be employed if chirality-controlled growth is to be observed in MD simulations. At present, our nonequilibrium carbon addition simulations are growing nanotubes 3 orders of magnitude faster than in experiment.

In the present simulation, the penetration of carbons into the inside of the iron cluster was rarely observed, indicating that carbon cap nucleation does not necessarily require volume diffusion of carbon into the iron cluster, nor surface carbide formation. The mechanism of sp^2-carbon network nucleation observed in the present work is rather close to that of fullerene nucleation.[13] This similarity was already speculated by Smalley and co-workers in 1996.[27] Thus, it is not surprising that SWNTs can be nucleated on materials other than metal particles, including SiO_2 nanoparticles[28] or the C face of the SiC (000−1) surface[29,30] (the weaker carbon−surface interaction on the Si face of SiC (0001) leads to graphene growth). Apparently, the metal particle plays a key role in differentiating the nucleation process from fullerene cage formation, by exhibiting "catalytic effects" that include (1) holding carbon fragments on the surface, (2) slowing down diffusion, (3) making the Fe−C bond the most reactive (keeping the carbon edge "alive"), (4) slowing down bond rearrangement processes, and (5) preventing closure of the curved open-ended carbon structure. Consequently, the metal−carbon adhesion strength is an important parameter influencing mechanism and growth efficiency, as has been discussed extensively in the literature.[12]

METHODS

Quantum chemical molecular dynamics (QM/MD) simulations were performed employing the self-consistent-charge density functional tight-binding method (SCC-DFTB)[17] with a finite electronic temperature approach.[31−33] In the present simulations, the electronic temperature was set to 0.86 eV, which corresponds to 10 000 K,[20] which allows smooth change in the occupancy of molecular orbitals around the Fermi level. We chose such a relatively large Fermi broadening because this energy roughly corresponds to the half-width of the 3d band of the Fe_{38} iron cluster, and we should be able to describe "an average" of many electronic states arising from d open shells of a large number of iron atoms. The use of electronic temperature also allows us to describe the multitude of electronic states associated with the dangling bonds on carbon. We found that a decrease of 1 order of magnitude in the electronic temperature significantly lowers the reactivity and structural fluctuation of the iron cluster, effectively slowing down carbon nucleation. In the molecular dynamics simulations, the velocity Verlet integrator was used with a time step of 2 fs (femtosecond; 10^{-15} s) for equilibration of a pure iron system, and 1 fs for metal−carbon systems. The nuclear temperature of the system was controlled at all times by the Nosé−Hoover chain thermostat.[34] Each 410 ps simulation took several months of wall-clock core time on the Fujitsu HX600 computer with 2.3 GHz AMD Opteron CPU. Graphical representation of the structures was obtained using the MacMolPlt software.[35]

Acknowledgment. This work was in part supported by a CREST (Core Research for Evolutional Science and Technology) grant in the Area of High Performance Computing for Multiscale and Multiphysics Phenomena from the Japan Science and Technology Agency (JST). S.I. also acknowledges support by the Program for Improvement of Research Environment for Young Researchers from Special Coordination Funds for Promoting Science and Technology (SCF) commissioned by the Ministry of Education, Culture, Sports, Science and Technology (MEXT) of Japan. The simulations were performed in part using the computer resources at Academic Center for Computing and Media Studies (ACCMS) at Kyoto University.

Supporting Information Available: Contents of four QuickTime movie files that show details of trajectories described in the text. This material is available free of charge *via* the Internet at http://pubs.acs.org.

REFERENCES AND NOTES

1. Kataura, H.; Kumazawa, Y.; Maniwa, Y.; Ohtsuka, Y.; Sen, R.; Suzuki, S.; Achiba, Y. Diameter Control of Single-Walled Carbon Nanotubes. *Carbon* **2000**, *38*, 1691–1697.
2. Fan, X.; Buczko, R.; Puretzky, A. A.; Geohegan, D. B.; Howe, J. Y.; Pantelides, S. T.; Pennycook, S. J. Nucleation of Single-Walled Carbon Nanotubes. *Phys. Rev. Lett.* **2003**, *90*, 145501.
3. Hofmann, S.; Csanyi, G.; Ferrari, A. C.; Payne, M. C.; Robertson, J. Surface Diffusion: The Low Activation Energy Path for Nanotube Growth. *Phys. Rev. Lett.* **2005**, *95*, 036101.
4. Harris, P. J. F. Solid State Growth Mechanisms for Carbon Nanotubes. *Carbon* **2007**, *45*, 229–239.
5. Amara, H.; Bichara, C.; Ducastelle, F. Understanding the Nucleation Mechanisms of Carbon Nanotubes in Catalytic Chemical Vapor Deposition. *Phys. Rev. Lett.* **2008**, *100*, 056105.
6. Hofmann, S.; Sharma, R.; Ducati, C.; Du, G.; Mattevi, C.; Cepek, C.; Cantoro, M.; Pisana, S.; Parvez, A.; Cervantes-Sodi, F.; Ferrari, A. C.; Dunin-Borkowski, R.; Lizzit, S.; Petaccia, L.; Goldoni, A.; Robertson, J. *In Situ* Observations of Catalyst Dynamics during Surface-Bound Carbon Nanotube Nucleation. *Nano Lett.* **2007**, *7*, 602–608.
7. Yoshida, H.; Takeda, S.; Uchiyama, T.; Kohno, H.; Homma, Y. Atomic-Scale *In-Situ* Observation of Carbon Nanotube Growth from Solid State Iron Carbide Nanoparticles. *Nano Lett.* **2008**, *8*, 2082–2086.

8. Shibuta, Y.; Maruyama, S. Molecular Dynamics Simulation of Formation Process of Single-Walled Carbon Nanotubes by CCVD Method. *Chem. Phys. Lett.* **2003**, *382*, 381–386.
9. Ding, F.; Bolton, K.; Rosen, A. Nucleation and Growth of Single-Walled Carbon Nanotubes: A Molecular Dynamics Study. *J. Phys. Chem. B* **2004**, *108*, 17369–17377.
10. Ding, F.; Bolton, K.; Rosen, A. Molecular Dynamics Study of SWNT Growth on Catalyst Particles without Temperature Gradients. *Comput. Mater. Sci.* **2006**, *35*, 243–246.
11. Bolton, K.; Ding, F.; Rosen, A. Atomistic Simulations of Catalyzed Carbon Nanotube Growth. *J. Nanosci. Nanotechnol.* **2006**, *6*, 1211–1224.
12. Ding, F.; Larsson, P.; Larsson, J. A.; Ahuja, R.; Duan, H.; Rosen, A.; Bolton, K. The Importance of Strong Carbon-Metal Adhesion for Catalytic Nucleation of Single-Walled Carbon Nanotubes. *Nano Lett.* **2008**, *8*, 463–468.
13. Irle, S.; Zheng, G.; Wang, Z.; Morokuma, K. The C60 Formation Puzzle "Solved": QM/MD Simulations Reveal the Shrinking Hot Giant Road of the Dynamic Fullerene Self-Assembly Mechanism. *J. Phys. Chem. B* **2006**, *110*, 14531–14545.
14. Gavillet, J.; Loiseau, A.; Journet, C.; Willaime, F.; Ducastelle, F.; Charlier, J.-C. Root-Growth Mechanism for Single-Wall Carbon Nanotubes. *Phys. Rev. Lett.* **2001**, *87*, 275504.
15. Raty, J. Y.; Gygi, F.; Galli, G. Growth of Carbon Nanotubes on Metal Nanoparticles: A Microscopic Mechanism from *Ab Initio* Molecular Dynamics Simulations. *Phys. Rev. Lett.* **2005**, *95*, 096103.
16. Porezag, D.; Frauenheim, T.; Kohler, T.; Seifert, G.; Kaschner, R. Construction of Tight-Binding-like Potentials on the Basis of Density-Functional Theory—Application to Carbon. *Phys. Rev. B* **1995**, *51*, 12947–12957.
17. Elstner, M.; Porezag, D.; Jungnickel, G.; Elsner, J.; Haugk, M.; Frauenheim, T.; Suhai, S.; Seifert, G. Self-Consistent-Charge Density-Functional Tight-Binding Method for Simulations of Complex Materials Properties. *Phys. Rev. B* **1998**, *58*, 7260–7268.
18. Zheng, G. S.; Witek, H. A.; Bobadova-Parvanova, P.; Irle, S.; Musaev, D. G.; Prabhakar, R.; Morokuma, K. Parameter Calibration of Transition-Metal Elements for the Spin-Polarized Self-Consistent-Charge Density-Functional Tight-Binding (DFTB) Method: Sc, Ti, Fe, Co, and Ni. *J. Chem. Theory Comput.* **2007**, *3*, 1349–1367.
19. Ohta, Y.; Okamoto, Y.; Irle, S.; Morokuma, K. Single-Walled Carbon Nanotube Growth From a Cap Fragment on an Iron Nanoparticle: Density-Functional Tight-Binding Molecular Dynamics Simulations. *Phys. Rev. B* **2009**, 195415.
20. Ohta, Y.; Irle, S.; Okamoto, Y.; Morokuma, K. Rapid Growth of a Single-Walled Carbon Nanotube On an Iron Cluster: Density-Functional Tight-Binding Molecular Dynamics Simulations. *ACS Nano* **2008**, *2*, 1437–1444.
21. Ohta, Y.; Okamoto, Y.; Irle, S.; Morokuma, K. Temperature Dependence of Iron-Catalyzed Continued Single-Walled Carbon Nanotube Growth Rates: Density Functional Tight-Binding Molecular Dynamics Simulations. *J. Phys. Chem. C* **2009**, *113*, 159–169.
22. Ohta, Y.; Okamoto, Y.; Irle, S.; Morokuma, K. Density-Functional Tight-Binding Molecular Dynamics Simulations of SWCNT Growth by Surface Carbon Diffusion on an Iron Cluster. *Carbon* **2009**, *47*, 1270–1275.
23. Zhang, Q. M.; Wells, J. C.; Gong, X. G.; Zhang, Z. Y. Adsorption of a Carbon Atom on the Ni-38 Magic Cluster and Three Low-Index Nickel Surfaces: A Comparative First-Principles Study. *Phys. Rev. B* **2004**, *69*, 205413.
24. Muller, M.; Erhart, P.; Albe, K. Analytic Bond-Order Potential For Bcc and Fcc Iron—Comparison with Established Embedded-Atom Method Potentials. *J. Phys.: Condens. Matter* **2007**, *19*, 326220.
25. Dinadayalane, T. C.; Sastry, G. N. Isolated Pentagon Rule in Buckybowls: A Computational Study on Thermodynamic Stabilities and Bowl-to-Bowl Inversion Barriers. *Tetrahedron* **2003**, *59*, 8347–8351.
26. Larsson, P.; Larsson, J. A.; Ahuja, R.; Ding, F.; Yakobson, B. I.; Duan, H. M.; Rosen, A.; Bolton, K. Calculating Carbon Nanotube−Catalyst Adhesion Strengths. *Phys. Rev. B* **2007**, *75*, 115419.
27. Thess, A.; Lee, R.; Nikolaev, P.; Dai, H. J.; Petit, P.; Robert, J.; Xu, C. H.; Lee, Y. H.; Kim, S. G.; Rinzler, A. G.; Colbert, D. T.; Scuseria, G. E.; Tomanek, D.; Fischer, J. E.; Smalley, R. E. Crystalline Ropes of Metallic Carbon Nanotubes. *Science* **1996**, *273*, 483–487.
28. Huang, S.; Cai, Q.; Chen, J.; Qian, Y.; Zhang, L. Metal-Catalyst-Free Growth of Single-Walled Carbon Nanotubes on Substrates. *J. Am. Chem. Soc.* **2009**, *131*, 2094–2095.
29. Kusunoki, M.; Suzuki, T.; Hirayama, M.; Shibata, N.; Kaneko, K. A Formation Mechanism of Carbon Nanotube Films on SiC(000−1). *Appl. Phys. Lett.* **2000**, *77*, 531–533.
30. Wang, Z.; Irle, S.; Zheng, G.; Kusunoki, M.; Morokuma, K. Carbon Nanotubes Grow on the C-Face of SiC (000−1) during Sublimation Decomposition: Quantum Chemical Molecular Dynamics Simulations. *J. Phys. Chem. C* **2007**, *111*, 12960–12972.
31. Weinert, M.; Davenport, J. W. Fractional Occupations and Density-Functional Energies and Forces. *Phys. Rev. B* **1992**, *45*, 13709–13712.
32. Wentzcovitch, R. M.; Martins, J. L.; Allen, P. B. Energy *versus* Free-Energy Conservation in 1st-Principles Molecular-Dynamics. *Phys. Rev. B* **1992**, *45*, 11372–11374.
33. Wagner, F.; Laloyaux, T.; Scheffler, M. Errors in Hellmann-Feynman Forces Due to Occupation-Number Broadening and How They Can Be Corrected. *Phys. Rev. B* **1998**, *57*, 2102–2107.
34. Martyna, G. J.; Klein, M. L.; Tuckerman, M. Nosé−Hoover Chains—The Canonical Ensemble *via* Continuous Dynamics. *J. Chem. Phys.* **1992**, *97*, 2635–2643.
35. Bode, B. M.; Gordon, M. S. MacMolplt: A Graphical User Interface for GAMESS. *J. Mol. Graphics Model.* **1998**, *16*, 133–138.